XL CILAMCE
IBERO-LATIN AMERICAN CONGRESS ON COMPUTATIONAL METHODS IN ENGINEERING
NOVEMBER 11-14, 2019
Praiamar Natal Hotel & Convention
Natal, RN-BRAZIL

NUMERICAL STUDY OF STEEL-CONCRETE COMPOSITE STRUCTURES UNDER FIRE SITUATION

Rafael C. Barros
rafael.barros@ufop.edu.br
Federal University of Ouro Preto
Campus Universitário s/n, Morro do Cruzeiro, 35400-000, Ouro Preto, MG, Brazil
Dalilah Pires
dalilah@ufsj.edu.br
Federal University of São João del-Rei
Campus Alto Paraopeba, Rod. MG 443, km 7, 36420-000, Ouro Branco, MG, Brazil
Ígor J.M. Lemes
igor.lemes@deg.ufla.br
Federal University of Lavras
Campus Universitário, 37200-000, Lavras, MG, Brazil
Ricardo A.M. Silveira
ricardo@em.ufop.br
Federal University of Ouro Preto
Campus Universitário s/n, Morro do Cruzeiro, 35400-000, Ouro Preto, MG, Brazil

Abstract. This work aims to study the behavior of steel-concrete composite structures under fire situation. For this, numerical formulations were developed, implemented and evaluated. It is well known that high temperature causes changes in physical properties and mechanical strength of materials. In both steel and concrete, such characteristics deteriorate during the exposure to fire, and the structure load capacity and stiffness are reduced significantly as a consequence of the temperature rises. This work shows the efficiency of the CS-ASA/FA and CS-ASA/FSA FE code in the analysis of steel-concrete composite structural elements. The first provide the temperature distribution at the cross-section level of the elements; the second module was developed to performs the inelastic second-order analysis of composite structures under fire using a large displacement FE co-rotational formulation; the plastic effects are captured through the refined plastic hinge method (RPHM) coupled to the strain compatibility method (SCM). The proposed numerical methodology success is proved by comparison with experimental and numerical responses available in the literature, which concludes that the developed computational tool can be used to study the composite steel-concrete cross-section strength and advanced progressive collapse analysis of beams, columns, arches and composite frames under fire.

Keywords: Thermal analysis, Thermo-structural analysis, Fire, MEF, CS-ASA.

**Acknowledgments from the authors to UFOP and CAPES for funding this work.*

1 Introduction

The use of composite steel-concrete structures is increasing because of the many advantages that this combination of materials provides. This constructive system allows the two materials to be used together in beams, columns, frames and slabs in order to obtain a structure with high structural performance, geometric precision and low on-site waste.

The building stability in a fire situation involves the knowledge of the consequences of rising temperatures in the structures, which has been achieved through laboratory experimentation and the use of increasingly sophisticated numerical models that allow a better understanding of the structural behavior under fire conditions [1]. For example, it is known that the high temperature in fires causes changes in the physical and mechanical characteristics of materials. In both steel and concrete, these characteristics deteriorate during fire exposure and the strength and stiffness of the structural elements are considerably reduced with increasing temperature.

Despite of the significant increase in the use of steel-concrete composite structures, research on the behaviour of these structures, especially in a fire situation, is still modest in Brazil. Thus, experimental studies and numerical models capable of simulating the behaviour of structures in fire situation becomes extremely relevant.

Shallal et al. [2] investigated the influence of high temperatures on continuous steel-concrete composite beams through an inelastic analysis. Their numerical models were based on a one-dimensional element of 4 nodes, with 3 degrees of freedom per node, including the partial interaction between the steel profile and the concrete slab. Good agreement was observed between their numerical results and the data from literature. Other recent works involving composite beams numerical analysis in fire situations can be cited, i.e.: Landesmann [3], Jiang et al. [4], Ahn and Lee [5] and Pak et al. [6].

The use of hollow structural steel sections is increasing and has several benefits: Such sections are very efficient structurally in resisting compression loads. By filling these sections with concrete, a substantial increase in load-bearing capacity can be achieved. Fire resistance can be obtained without the necessity of external fire protection for the steel, and eliminating steel surface protection increases the usable space in a building.

Espinos et al. [7] presented the results of a numerical investigation on strategies for enhancing the fire behaviour of concrete-filled steel tubular (CFST) columns by using inner steel profiles as circular hollow sections (CHS), HEB profiles or embedded steel core profiles. The ABAQUS commercial software was adopted, and a 3D finite element that allowed to compute different sections and nonlinear materials behavior under high temperatures was considered. Parametric studies were developed with the purpose of investigating the cross-section geometry influence on the resistant capacity of the columns under fire. Regarding the study of CFST columns can be cited: Dai and Lam [8], Rodrigues et al. [9], Kamil et al. [10] and Zhou et al. [11].

The objective of this work is to apply the in-house developed CS-ASA/FA (Computational System for Advanced Structural Analysis/Fire Analysis) and CS-ASA/FSA (Fire Structural Analysis) computational modules to the steel-concrete composite structural elements, such as beams and columns, in fire situation. The first provide the temperature distribution at the cross-section level of the elements; the second module was developed for the inelastic second-order analysis of structures submitted to high temperatures. An approach based on the Strain Compatibility Method (SCM) is proposed to evaluate the cross-section strength level and the axial and bending stiffness of the composite structures under high temperatures. The construction of the moment-curvature relationship is essential for this evaluation. The tangent of the moment-curvature relationship, the stiffness, depends only on the chosen material behavior of the constituents. This methodology is coupled to the Refined Plastic Hinge Method (RPHM), in which the plasticity is evaluated only in the element nodal points using generalized stiffness parameters [12]. Figure 1 illustrates the coupling between the SCM and the RPHM.

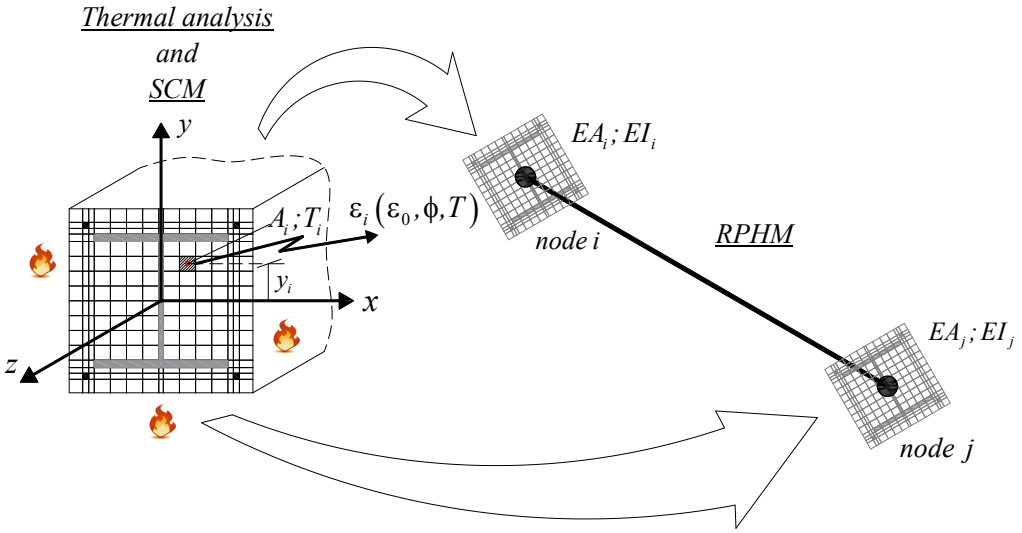

Figure 1. SCM and RPHM coupling

2 Thermal analysis

For a given composite steel-concrete cross-section, the finite element thermal analysis is performed by solving the 2-D heat conduction equation:

$$\mathbf{C}\dot{\mathbf{T}} + \mathbf{K}\mathbf{T} = \mathbf{R} \tag{1}$$

in which, $\mathbf{C} = \int_\Omega \rho c \mathbf{N}^T \mathbf{N} d\Omega$ is the capacitance matrix (thermal capacity);

$\mathbf{K} = \int_\Omega \mathbf{B}^T \mathbf{D} \mathbf{B} d\Omega + h\int_\Gamma \mathbf{N}^T \mathbf{N} d\Gamma$ is the thermal conductivity matrix;

$\mathbf{R} = Q\int_\Omega \mathbf{N}^T d\Omega + hT_\infty \int_\Gamma \mathbf{N}^T d\Gamma - q_0 \int_\Gamma \mathbf{N}^T d\Gamma$ is the nodal heat flux vector; and

T is the nodal temperatures vector meant to be determined. The matrices **N**, **B**, and **D** are the matrix of interpolation functions, the matrix that contains the derivatives with respect to x and y of the interpolation functions, and the matrix containing the thermal conductivities, respectively; ρ is the unit material mass, c is the specific heat of the material; h is the coefficient of heat transmission by convection and/or by radiation; T_∞ is the gases temperature; q_0 is the heat flux prescribed at time t; and Q is the heat generated inside the element per unit volume and time.

The cross-section thermal analysis can be made using four types of two-dimensional finite elements: two triangular elements T3 and T6, with 3 and 6 nodes, respectively; and two quadrilateral elements Q4 and Q8, with 4 and 8 nodes, respectively.

To obtain the solution of Eq. (1) an explicit numerical time integration strategy based on the finite difference method is adopted [13]. Since the Eq. (1) is strongly nonlinear due to the dependence of the material properties on temperature some incremental or incremental-iterative strategies have to be considered in solving the nonlinear system. In the proposed approach a simple incremental procedure has been applied, which is detailed in Table 1.

In Table 1, n represents the time step; t_0 and T_0 are the first time step and temperature vector in the first time step, respectively; and θ is the parameter that defines the instant at which the equation illustrated in step 2e is satisfied.

Table 1. Simple incremental algorithm

1. Solution of the heat transfer transient problem:
1a. Sets input data, initial and boundary conditions
1b. Do: $T_n = T_{n+1} = T_0 = 20°C$
2. Incremental process: *inc* = 1, 2, 3,..., *nmax*
2a. Calculate the capacitance matrix: $\mathbf{C} = \int_\Omega \rho c \mathbf{N}^T \mathbf{N} d\Omega$
2b. Calculate thermal conductivity matrix: $\mathbf{K} = \int_\Omega \mathbf{B}^T \mathbf{D} \mathbf{B} d\Omega + h \int_\Gamma \mathbf{N}^T \mathbf{N} d\Gamma$
2c. Calculates the heat flux vector: $\mathbf{R} = Q \int_\Omega \mathbf{N}^T d\Omega + h T_\infty \int_\Gamma \mathbf{N}^T d\Gamma - q_0 \int_\Gamma \mathbf{N}^T d\Gamma$
2d. Get: $\hat{\mathbf{K}} = \left(\mathbf{C} + \theta \Delta t \mathbf{K} \right)$
2e. Get: $\hat{\mathbf{R}} = \left[\mathbf{C} - (1-\theta) \Delta t \mathbf{K} \right] \mathbf{T}_n + \Delta t \left[\theta \mathbf{R}_{n+1} + (1-\theta) \mathbf{R}_n \right]$
2f. Solve the system of equations: $\mathbf{T}_{n+1} = \hat{\mathbf{K}}^{-1} \hat{\mathbf{R}}$
3. Give a new time increment and go to step 2

3 Structural analysis

The steel-concrete composite structures inelastic behavior in fire condition is captured using the RPHM and SCM coupling [12]. The thermal action effects on the structure, i.e., the material stiffness and yield strength degradations, as well as the influence of the thermal strain on the element cross-section were considered within these numerical approaches. The following sections bring a summary of the FE formulation via RPHM, the SCM and how the bending moment-curvatures relationships are derived. Additional details of the structural solution strategy can be found in Pires [14] and Barros et al. [13].

3.1 Finite element formulation via RPHM

The objective of the RPHM is to capture the evolution of the plastification at the nodes of the element, from the beginning of the yielding to its total plastification with a plastic hinge formation. The following main assumptions are considered in the model: all finite elements are initially straight and prismatic and their cross-sections remain plane after deformation; the steel profiles are compact; rigid body large displacements and rotations are represented; the shear deformation effects are ignored. The developed finite element is delimited by nodal points *i* and *j*, as illustrated in Fig. 2. P, M_i, M_j and δ, θ_i, θ_j are the internal forces and associated displacements in the co-rotational system, respectively.

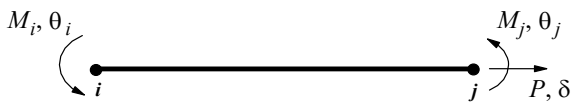

Figure 2. Beam-column finite element

The incremental equilibrium relationship of the finite element illustrated in Fig. 2 is given by:

$$\begin{Bmatrix} \Delta P \\ \Delta M_i \\ \Delta M_j \end{Bmatrix} = \begin{bmatrix} k_{11} & 0 & 0 \\ 0 & k_{22} & k_{23} \\ 0 & k_{32} & k_{33} \end{bmatrix} \begin{Bmatrix} \Delta \delta \\ \Delta \theta_i \\ \Delta \theta_j \end{Bmatrix} \tag{2}$$

in which Δ denotes the increments of each quantity. The terms related to flexural stiffness in the matrix depend on geometric nonlinearity. A simplified second-order formulation, presented by Yang

and Kuo [15] was adopted here. Implementation details are available in Lemes [12] and Lemes et al. [16].

3.2 Strain compatibility method (SCM)

When under external loads, a structure deforms to reach equilibrium. On the cross-section level, once the generalized internal forces equal the generalized external forces, the deformation stops [16]. This cross-section deformation is addressed in the SCM. For the application of this method, it is assumed that the strain field is linear and the section remains plane after deformation (Fig. 3). This method couples the cross-section deformed configuration to the constitutive relationship of the material composing it.

The evaluation of the axial and flexural stiffnesses is derived from the moment-curvature relationship and depends on the modulus of elasticity, which is obtained from the material (steel and concrete) constitutive relations [14].

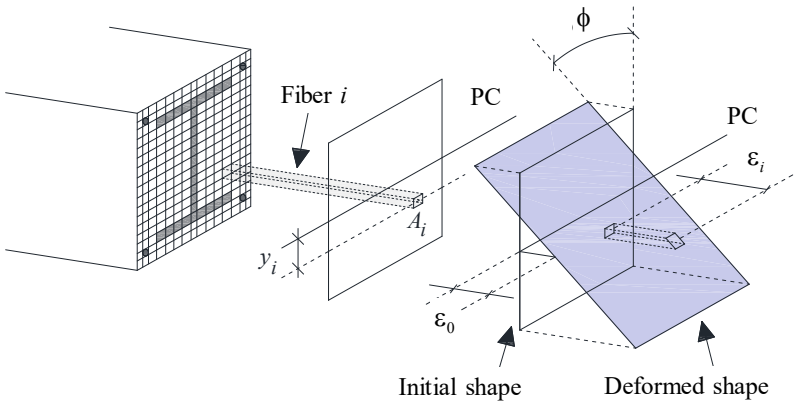

Figure 3. Linear strain field

3.3 Moment-curvature relationship

A discretization of the cross-section into fibers is performed with the objective of describing the deformation distribution using the axial strain (ε_i) in the plastic centroid (PC) of each fiber. From this the stress (σ_i) in each fiber is computed through the constitutive relationships of the materials. The axial strain in the i^{th} fiber is given by:

$$\varepsilon_i = \varepsilon_0 + \phi y_i \tag{3}$$

where y_i is the distance between the plastic centroids of the fiber analyzed and the cross-section; ε_0 is the axial strain at the PC of the section; and ϕ is the respective curvature.

The Newton-Raphson method is used at the cross-section level in order to obtain the moment-curvature relationship (M - ϕ). In matrix notation, the variables ε_0 and ϕ are components of the generalized strain vector $\mathbf{X} = [\varepsilon_0 \ \phi]^T$. For computing the axial and flexural generalized stiffness, $\mathbf{X} = \mathbf{0}$ is adopted in the first iteration, so that convergence is reached quickly [17]. It can be said that the cross-section equilibrium is obtained when the following equation is satisfied:

$$\mathbf{F}(\mathbf{X}) = \mathbf{f}_{ext} - \mathbf{f}_{int} = \begin{bmatrix} N_{ext} \\ M_{ext} \end{bmatrix} - \begin{bmatrix} N_{int} \\ M_{int} \end{bmatrix} < tol \tag{4}$$

where $\mathbf{f}_{ext}$ is the external force vector given by the axial force N_{ext} and bending moment M_{ext}; the terms N_{int} and M_{int} are the components of the internal force vector, $\mathbf{f}_{int}$ and *tol* is a tolerance.

The internal forces are obtained from the deformed configuration of the cross-section through the expressions:

$$N_{int} = \iint_{A_a} \sigma_a dA + \iint_{A_c} \sigma_c dA + \iint_{A_b} \sigma_b dA \cong \sum_{i=1}^{n_{fib,a}} \sigma_{ai} A_{ai} + \sum_{i=1}^{n_{fib,c}} \sigma_{ci} A_{ci} + \sum_{i=1}^{n_{fib,b}} \sigma_{bi} A_{bi} \tag{5}$$

$$M_{int} = \iint_{A_a} \sigma_a y dA + \iint_{A_c} \sigma_c y dA + \iint_{A_b} \sigma_b y dA \cong \sum_{i=1}^{n_{fib,a}} \sigma_{ai} A_{ai} y_{ai} + \sum_{i=1}^{n_{fib,c}} \sigma_{ci} A_{ci} y_{ci} + \sum_{i=1}^{n_{fib,b}} \sigma_{bi} A_{bi} y_{bi} \tag{6}$$

where $n_{fib,a}$ is the number of fibers; σ_a, σ_c and σ_b are the stress in steel, concrete and steel rebar, respectively; A_i and y_{ai} are the i^{th} fiber area and its positions in relation to the Plastic Neutral Axis (PNA), respectively.

For the following iteration, k+1, the strain vector is calculated according to [17]:

$$\mathbf{X}^{k+1} = \mathbf{X}^k + \mathbf{F}'\left(\mathbf{X}^k\right)^{-1} \mathbf{F}\left(\mathbf{X}^k\right) \tag{7}$$

where $\mathbf{F}'$ is the Jacobian matrix for the non-linear problems, i.e.:

$$\mathbf{F}' = \left(\frac{\partial \mathbf{F}}{\partial \mathrm{x}}\right) = \begin{bmatrix} \dfrac{\partial N_{int}}{\partial \varepsilon_0} & \dfrac{\partial N_{int}}{\partial \phi} \\ \dfrac{\partial M_{int}}{\partial \varepsilon_0} & \dfrac{\partial M_{int}}{\partial \phi} \end{bmatrix} \tag{8}$$

This numerical procedure is adapted and used for obtaining the N-M interaction curves as well. For a given axial force, the limit moment from the relationship of the moment-curvature is obtained, corresponding to the cross-section total plastification. This pair of forces define a point on the N-M interaction diagram. Noteworthy is the fact that the interaction curves are obtained independently the structural analysis, i.e. computed beforehand, in order to accelerate the execution of the structural simulations. More details on the computation of interaction curves, the structural analysis, as well as the thermal structural problem, can be found in Lemes [12], Barros et al. [13] and Pires [14].

3.4 Thermally induced strains

The thermal action effects on the structure, i.e., the stiffness and material and yield strength degradations, as well as the influence of the thermal strain on the element cross-section were considered within the numerical approaches shown in Section 3. However, in the approach used here, the total strains are replaced by mechanical strains. Thus, the axial strain in the i^{th} fiber is determined by:

$$\varepsilon_{mec,i} = \varepsilon_{tot} - \varepsilon_{th} \tag{9}$$

with ε_{tot} is the total strain and ε_{th} the thermal strain, computed as shown in EC 4 part 1-2 [18] for concrete and steel. The transient and creep strains in concrete were neglected.

4 Numerical analysis

4.1 Structural behaviour of isolated beams

Landesmann [3] presented the numerical results of two simply supported steel-concrete composite beams in fire conditions. From this study, two different cross-sections configurations were verified: (*i*) composite beam denoted as CB1, and (*ii*) composite partially encased beam, denoted as CB2. The general configuration of the proposed sections is given by Fig. 4. Both composite beams (CB1 and CB2) are constituted of a W310x31 steel section, made with ASTM A572-gr50 steel grade (f_{yk} = 345 N/mm²) connected to a 100 mm thick C20 concrete slab (f_{ck} = 20 N/mm²).

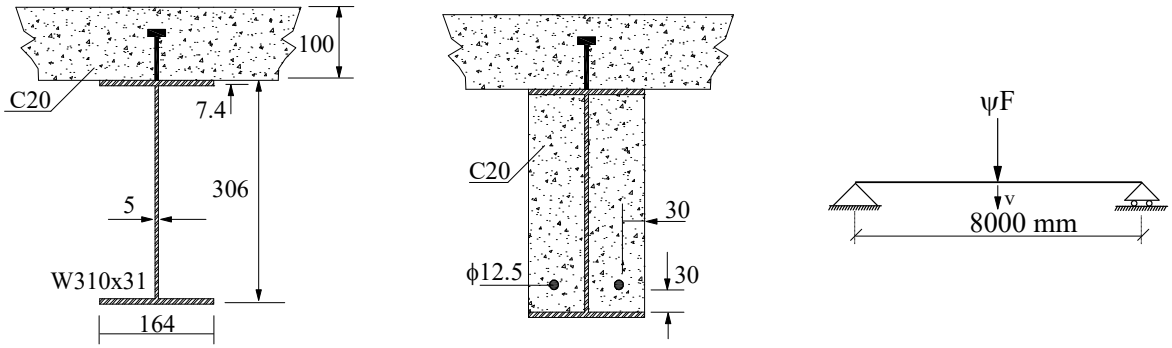

a) CB1 (mm) b) CB2 (mm) c) Loading point

Figure 4. Loading and geometry

The full composite behaviour, i.e. interaction between steel and 1250 mm effective slab, is assured by steel stud bolts connectors. For composite CB2 case, a partially encased C20 concrete casting and two reinforcement steel bars of 12.5 mm of diameter (steel f_{yk} = 500 N/mm²) are also considered on the section design.

For each cross-section configuration, three different loading conditions, corresponding to ψ = 60 and 80% of the section ultimate bending moment capacity for ambient temperature ($M_{u,20}$), are assumed to occur simultaneously to a standard fire-design curve [19]. In this analysis, a two-step loading strategy is performed, in which an initial mid-span vertical nodal force F is firstly applied to the member, and kept constant at the required value ($\psi \cdot M_{u,20}$), whilst the external temperature (from the standard fire-design curve) is continuously incremented until no numerical convergence is obtained, which is interpreted as the member failure. Fire is supposed to occur on the bottom side of the member. As a result, only 3 sides of the section are engulfed by the flames. All thermal and mechanical parameters were considered according to EC 4 part 1-2 [18].

For the thermal analysis the cross-sections have been discretized into 105 and 249 quadrilateral finite elements with 4 nodes, respectively for CB1 and CB2 composite configurations. For thermo-structural analysis the proposed isolated beam members have been discretized into 8 beam-columns segments.

The temperature evolution obtained by CS-ASA/FA, as a function of the fire elapsed-time, were compared to those presented by Landesmann [3], showing a good agreement for the both cases, and can be seen in Fig. 5.

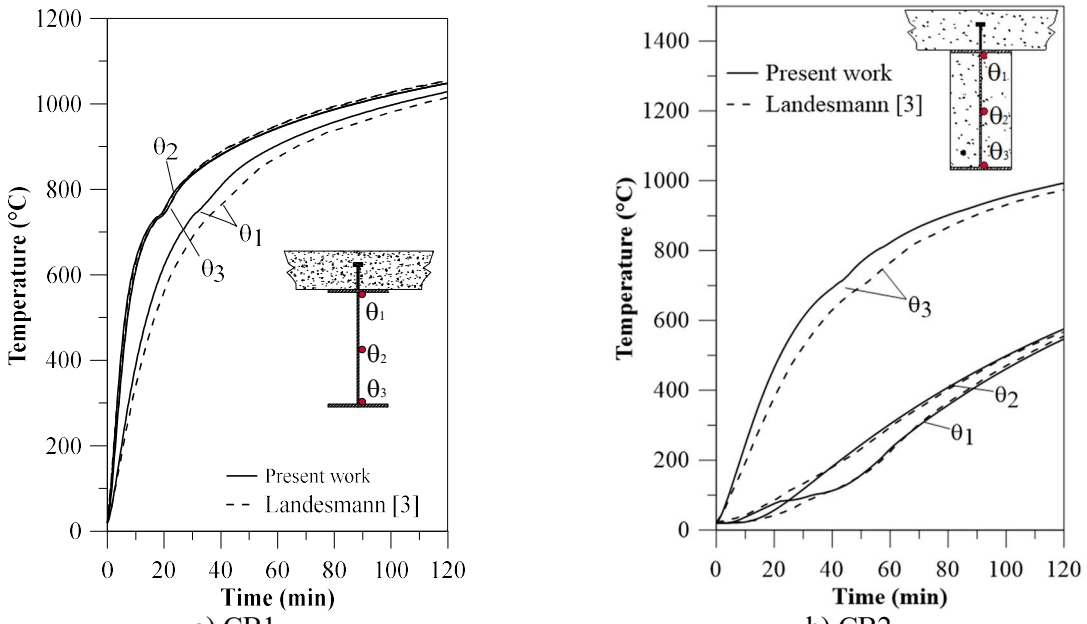

a) CB1 b) CB2

Figure 5. Curve Temperature versus Time for both composite beams

The room temperature structural analysis results, seeking to determine the beams critical load, as well as the interaction diagram between axial force and bending moment (N-M) for $t = 0$, are shown in Fig. 6. Figures 7a and 7b present the mid-span deflection *versus* time of the beams computed by CS-ASA/FSA, together with the numerical results of Landesmann [3]. The results were less conservative and reasonable when compared to the literature, especially when observing the point that determines the failure of the structural system.

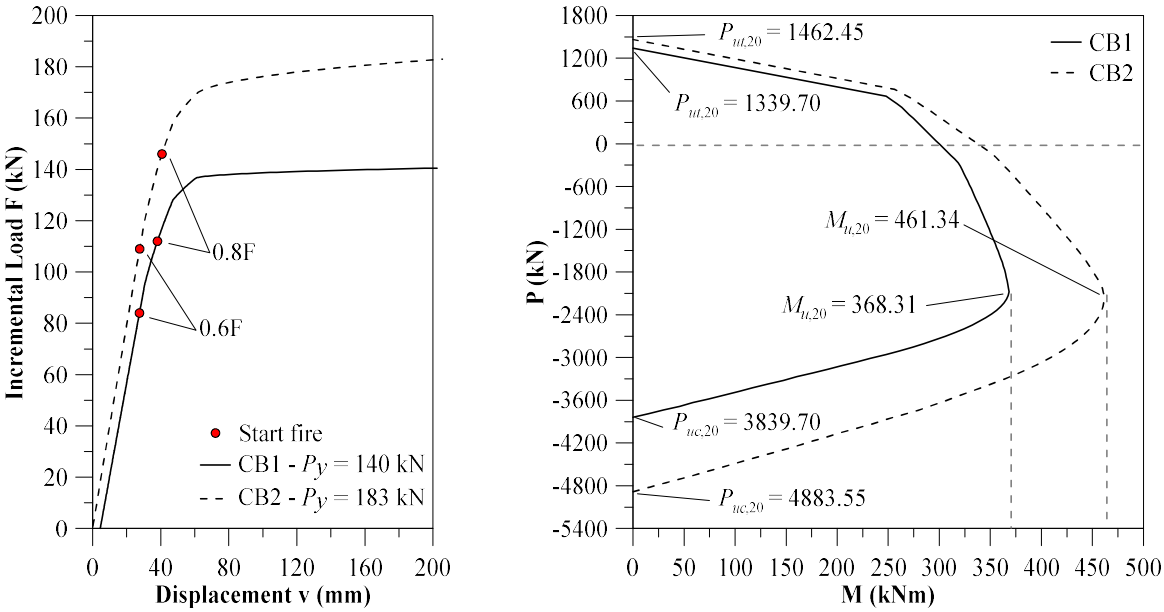

a) Equilibrium path b) Interaction diagram at room temperature

Figure 6. Room temperature structural analysis results of the composite beams

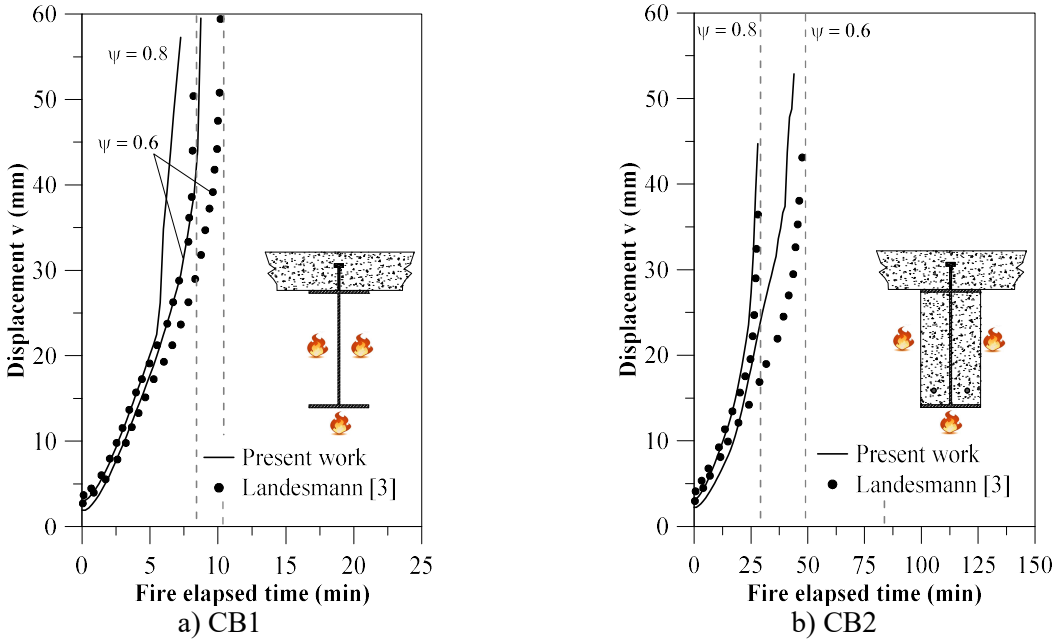

a) CB1 b) CB2

Figure 7. Fire structural analysis results of composite beams

4.2 Structural behaviour of isolated circular concrete-filled steel tubular column

Lie [20] and Kodur [21] presented an experimental study of circular concrete-filled steel tubular column (CFST), with an external diameter of 273 mm and a thickness equal to 6.35 mm. In Sousa Jr. et al. [22] the interaction diagrams between axial force and bending moment (N-M) for different time

intervals can be seen, and in Caldas [23] the numerical results of the thermal and thermo-structural analysis via MEF of this same column are presented.

In the thermal analysis the temperatures were evaluated at the surface of the steel tubular section and at the depths of 65 and 130 mm in the concrete. The upper limit of thermal conductivity was considered for concrete with calcareous aggregates and the other thermal properties according to EC 2 part 1-2 [24]. The heating rate was adopted based on the standard ASTM E119 [25] fire curve and, according to the literature, a moisture content of 10% relative to the concrete weight. The results obtained from nonlinear thermal simulation via CS-ASA/FA module are presented in Fig. 8a. A discretization with 1442 4-node quadrilateral elements (Q4) was adopted, and the temperature was evaluated at the same cross-sectional points selected by Lie [20]. The numerical results obtained in this research converge satisfactorily to those extracted from the literature (experimental and numerical).

For the construction of N-M interaction curves, Sousa Jr. et al. [22] considered the yield strength of steel equal to 350 MPa, concrete with compressive strength of 47 MPa and four reinforcement bars of diameter 19.5 mm and yield strength equal to 400 MPa are embedded in the concrete, with 23 mm of concrete cover. For this section, in order to obtain its N-M interaction diagrams, 427 quadrilateral finite element (Q4) and the standard ASTM E119 [25] fire curve for gas temperature have been adopted. These curves were computed for a time of 0, 30, 60 and 120 min of fire exposure, as shown in Figure 8b, using the results of Sousa Jr. et al. [22] for validation of those found through CS-ASA/FSA.

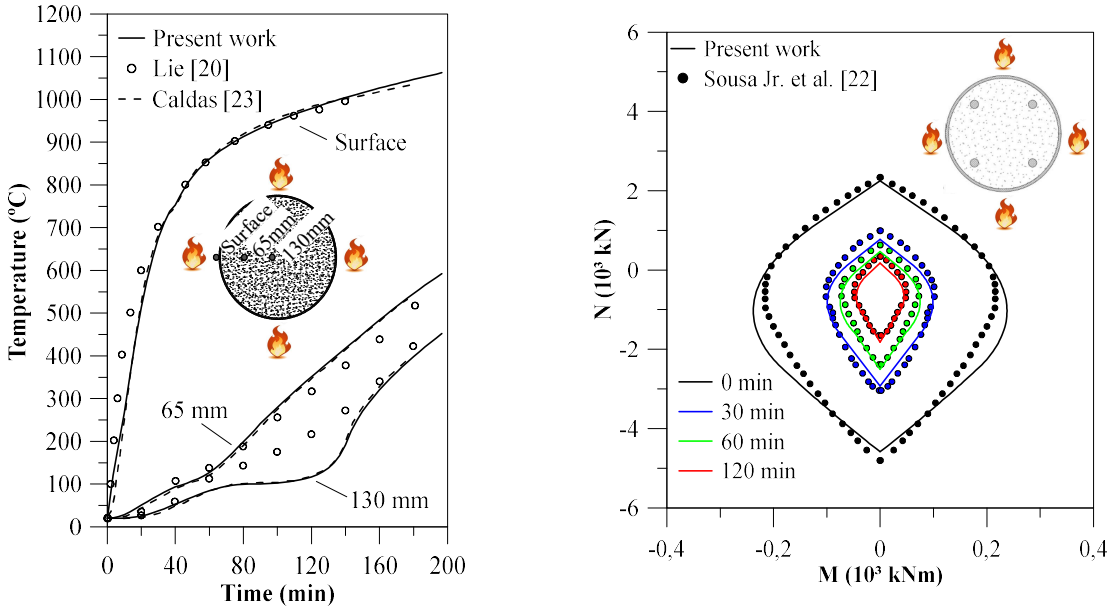

a) Temperatures at various depths of column b) N-M interaction diagrams

Figure 8. a) Thermal analysis results and b) N-M interaction diagrams for different time intervals

Kodur [21] showed the results of tests on concrete-filled tubular steel columns subjected to centered axial load, while Caldas [23] presented numerical results from one of these columns observed by Kodur [21]. The column in question has the same cross-section as previously shown, disregarding the reinforcement bars, and a length of 3810 mm subject to a centered axial load of 712 kN. Six beam-column elements were used to analyze the length of the column exposed to standard ASTM E119 [25] fire curve. The cross-section was discretized with 427 quadrilateral finite elements (Q4) and a sinusoidal imperfection of maximum amplitude equal to 0.1 mm was considered. In general, the moisture content was considered 4% and the material properties follow EC 4 part 1-2 [18]. Figure 9a illustrates the equilibrium path at room temperature, boundary and loading conditions of the structural system. Figure 9b shows a reasonable approximation of the results when compared to the literature, especially the experimental results, with emphasis on the point that configures the structure collapse.

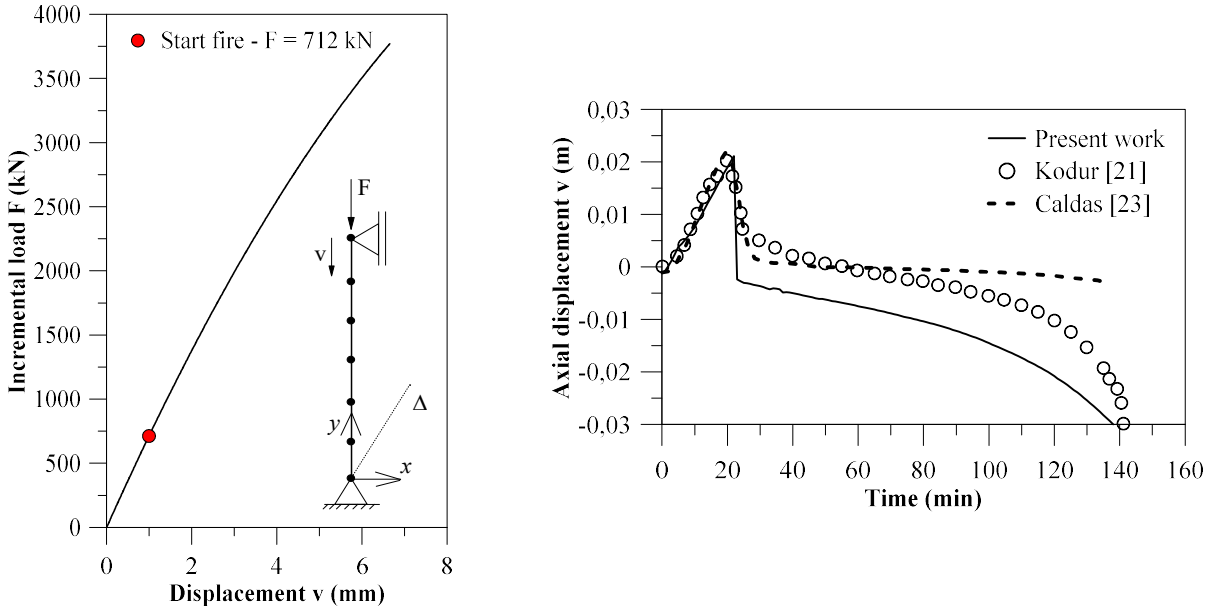

a) Equilibrium path b) Displacement versus time

Figure 9. Fire structural analysis results of CFST column

Figure 9b shows the typical axial displacement of unprotected columns. During the first stages of heating, the steel section resists most of the load due to its greater expansion compared to the concrete component of the composite section. As the temperature rises, the steel profile yield due to decreased strength and the column generally contracts for a standard fire exposure time of between 15 and 30 min. Due to the low conductivity of concrete, it loses strength more slowly than the profile, providing a fire resistance in later stages. When the concrete can no longer withstand loading, the column fails by crush or buckle. The time during which the concrete component can withstand loading can be quite significant as shown in Fig. 9b.

The present work predicts reasonably well the column behaviour, however, it should be noted the pronounced steel failure between 20 to 25 min of fire exposure and a divergence in results of approximately 1 cm from 25 min of analysis. Additionally, it is noteworthy that the proposed model captures well the column behaviour throughout the all analysis, with emphasis on the structure fails that occurs near 140 min of exposure.

5 Final remarks

The present study applied the CS-ASA/FA and CS-ASA/FSA computational modules to steel-concrete composite structural elements in fire situation, respectively. This modules efficiency had already been tested with steel and reinforced concrete structural elements in fire situations, where good results in both cases were observed in Barros et al. [13] and Pires [14].

The first numerical analysis consisted of composite beams subjected to thermal gradients. In general, the results obtained by both modules, CS-ASA/FA and CS-ASA/FSA, showed good agreement with those found in literature. However, it is noteworthy that, in the structural analysis in fire situation, it is possible to evidence a greater loss of stability in the proposed model, which may be related to the flexural stiffness coefficient determination and its degradation during the analysis.

Regarding the CFST column, the results obtained through the CS-ASA/FA showed once again a good convergence when compared to the numerical and experimental results illustrated in the literature. For the N-M interaction curves, the results obtained in this work were slightly less conservative when compared to those computed by Sousa Jr. et al. [22], considering all evaluated time intervals. The thermo-structural analysis performed by the CS-ASA/FSA module was also satisfactory, especially in determining the structure collapse time.

As a final conclusion, it is possible to affirm that the computational implementations, for thermal

and thermo-structural analysis of steel-concrete composite structural elements under fire were successfully performed and yield satisfactory results, capturing well the temperature elevation and the composite structures behaviour under high temperatures.

Acknowledgements

The authors would like to thank CAPES and CNPq (Federal Research Agencies), FAPEMIG (Minas Gerais Research Agency), Gorceix Foundation and UFOP/PROPP for their support during the preparation of this research work.

References

[1] R. C. Barros. Advanced numerical evaluation of steel structures performance under high temperatures. MSc, Federal University of Ouro Preto, 2016, (in Portuguese).
[2] M. A. Shallal and A. M. Almusawi. Non-linear analysis of continuous composite beams subjected to fire. *International Journal of Civil Engineering and Technology*, vol. 9, pp. 521-532, 2018.
[3] A. Landesmann. Refined plastic-hinge model for analysis of steel-concrete structures exposed to fire. *Journal of Constructional Steel Resear*ch, vol. 71, pp. 202-209, 2012.
[4] J. Jiang, G-Q. Li and A. Usmani. Analysis of composite steel-concrete beams exposed to fire using OpenSees. *Journal of Structural Fire Engineering*, vol. 6, pp. 1-19, 2015.
[5] J. K. Ahn and C. H. Lee. Fire behavior and resistance of partially encased and slim-floor composite beams. *Journal of Constructional Steel Research*. Vol. 129, pp. 276-285, 2016.
[6] H. Pak, M. S. Kang, J. W. Kang, S. H. Kee and B. J. Choi. A numerical study on the thermo-mechanical response of a composite beam exposed to fire. *International Journal of Steel Structures*, vol. 18(4), pp. 1177-1190, 2018.
[7] A. Espinos, M. L. Romero and D. Lam. Fire performance of innovative steel-concrete composite columns using high strength steels. *Thin-Walled Structures*, vol. 106, pp. 113-128, 2016.
[8] X. H. Dai, D. Lam. Shape effect on the behaviour of axially loaded concrete filled steel tubular stub columns at elevated temperature. *Journal of Constructional Steel Resear*ch, vol. 73, pp. 117-127, 2012.
[9] J. P. C. Rodrigues, A. J. M. Correia and T. A. C. Pires. Behaviour of composite columns made of totally encased steel sections in fire. *Journal of Constructional Steel Resear*ch, vol 105, pp. 97-106, 2015.
[10] G. M. Kamil, Q. Q. Liang and M. N. S. Hadi. Numerical analysis of axially loaded rectangular concrete-filled steel tubular short columns at elevated temperatures. *Engineering Structures*, vol. 180, pp. 89-102, 2019.
[11] X. Zhou, W. Wang, K. Song and Y. F. Chen. Fire resistance studies on circular tubed steel reinforced concrete stub columns subjected to axial compression. *Journal of Constructional Steel Resear*ch, vol 159, pp. 231-244, 2019.
[12] I. J. M. Lemes. Advanced numerical study of steel, concrete and steel-concrete composite structures. PhD thesis, Federal University of Ouro Preto, 2018, (in Portuguese).
[13] R. C. Barros, D. Pires, R. A. M. Silveira, I. J. M. Lemes and P. A. S. Rocha. Advanced inelastic analysis of steel structures at elevated temperatures by SCM/RPHM coupling. *Journal of Constructional Steel Research*, vol. 145, pp. 368-385, 2018.
[14] D. Pires. Advanced numerical analysis of steel and reinforced concrete structures in fire situation. PhD thesis, Federal University of Ouro Preto, 2018, (in Portuguese).
[15] Y. B. Yang and S. B. Kuo. *Theory and Analysis of Nonlinear Framed Structures*. Prentice Hall, 1994.
[16] I. J. M. Lemes, A. R. D. Silva, R. A. M. Silveira and P. A. S. Rocha. Nonlinear analysis of two-dimensional steel, reinforced concrete and composite steel concrete structures via coupling SCM/RPHM. *Engineering Structures*, vol. 147, pp. 12-26, 2017.
[17] C. G. Chiorean. A computer method for nonlinear inelastic analysis of 3D composite steel-concrete frame structures. *Engineering Structures*, vol. 57, pp. 125-152, 2013.

[18] European Committee for Standardization - EN 1994-1-2:2005. Eurocode 4: *Design of composite steel and concrete structures, Part 1-2: General rules, Structural Fire Design*.
[19] ISO 834-1. *Fire resistance tests - elements of buildings construction*, Part 1: General requirements. ISO - International Organization for Standardization. Geneva, 1999.
[20] T. T. Lie. Fire resistance of circular steel columns filled with bar-reinforced concrete. *Journal of Structural Engineering*, vol. 120, pp. 1489-1509, 1994.
[21] V. R. Kodur. Solutions for enhancing the fire endurance of HSS columns filled with high strength concrete. AISC, *Engineering Journal*, 1-7, 2006.
[22] J. B. M. Sousa Jr., R. B. Caldas, R. H. Fakury, 2009. Interaction diagrams for concrete-filled tubular sections under fire. *Tubular Structures XII: Proceedings of Tubular Structures*, China.
[23] R. B. Caldas. Numerical analysis of steel, concrete and composite structures subjected to fire. PhD thesis, Federal University of Minas Gerais, 2008.
[24] European Committee for Standardization - EN 1992-1-2:2004 Eurocode 2: *Design of Concrete Structures. Part 1-2: General rules, Structural Fire Design*.
[25] ASTM E119. *Standard test methods for fire test of building construction and materials*. Pennsylvania: American Society for Testing and Materials, 2008.